Harnessing Dynamical Encircling of an Exceptional Point in Anti-$\mathcal{PT}$-Symmetric Integrated Photonic Systems

Ziyao Feng and Xiankai Sun*
Department of Electronic Engineering, The Chinese University of Hong Kong, Shatin, New Territories, Hong Kong

(Received 11 May 2022; accepted 6 October 2022; published 28 December 2022)

Dynamically encircling an exceptional point in a non-Hermitian system can lead to chiral behaviors, but this process is difficult for on-chip $\mathcal{PT}$-symmetric devices which require accurate control of gain and loss rates. Here, we experimentally demonstrated encircling an exceptional point with a fixed loss rate in a compact anti-$\mathcal{PT}$-symmetric integrated photonic system, where chiral mode switching was achieved within a length that is an order of magnitude shorter than that of a $\mathcal{PT}$-symmetric system. Based on the experimental demonstration, we proposed a topologically protected mode (de)multiplexer that is robust against fabrication errors with a wide operating wavelength range. With the advantages of simplified fabrication and characterization processes, the demonstrated system can be used for studying higher-order exceptional points and for exotic light manipulation.

DOI: 10.1103/PhysRevLett.129.273601

Introduction.—It is well known that a non-Hermitian system under the parity–time ($\mathcal{PT}$) symmetry can have real eigenvalues [1]. A $\mathcal{PT}$-symmetric system may work in the $\mathcal{PT}$-unbroken or $\mathcal{PT}$-broken phase with real and complex eigenvalues, respectively, and the two phases are separated by an exceptional point (EP). The unique properties of $\mathcal{PT}$-symmetric systems have enabled interesting applications and phenomena such as unidirectional reflection [2,3], EP-enhanced sensing [4–7], and single-mode lasing [8,9]. Among all these applications, those based on EPs have drawn a lot of attention due to the EP's degeneracy of eigenvalues [5]. The topological features of the energy Riemann surface and EPs were also analyzed both theoretically and experimentally [10–16], which revealed that adiabatically varying the system's parameters around the EP in spatial or time domain can flip the eigenstates resulting in the initial eigenstate switched to another eigenstate. Such systems exhibit chiral dynamics in their eigenstates where the final state is determined by the encircling direction rather than the initial state, which has further led to applications such as asymmetric switching and nonreciprocal transmission. The chiral dynamics has been demonstrated on optical and microwave platforms [11,12]. The process of encircling higher-order EPs has also been theoretically analyzed and experimentally demonstrated for the topological study of complex non-Hermitian systems [17,18].

Previous theories and experiments have shown that $\mathcal{PT}$-symmetric systems can have nontrivial properties, which lead to unique applications in sensing, lasing, and energy transferring or harvesting. Those unconventional properties inspired the proposal of another type of non-Hermitian systems with real eigenvalues, known as "anti-$\mathcal{PT}$-symmetric (APT-symmetric) systems" [19]. The Hamiltonian of an APT-symmetric system switches to the opposite one under the joint operation of parity and time reversal. APT-symmetric systems have drawn wide attention with experimental demonstrations in diffusive systems [20], atomic systems [21], and electronic systems [22]. In contrast to $\mathcal{PT}$-symmetric optical systems that require the imaginary part of the refractive index (the gain or loss rate) to be changed, APT-symmetric optical systems only require a variation of the real part of the refractive index. Because of the less stringent requirements, the research of APT-symmetric systems has been extended to the areas of optics and photonics [23–25]. Similar to $\mathcal{PT}$-symmetric systems, APT-symmetric systems also have APT-unbroken and APT-broken phases that are separated by an EP. Therefore, many EP-based applications, e.g., encircling of EPs, can also work well in an APT-symmetric system. However, little attention has been paid to dynamically encircling an EP in an on-chip APT-symmetric photonic system.

In this Letter, we theoretically analyzed and experimentally demonstrated dynamically encircling an EP in an on-chip APT-symmetric optical waveguide system, where we observed the chiral behavior in the communication band with a wide wavelength range (∼100 nm). Different from $\mathcal{PT}$-symmetric systems which require the initial state to be an eigenstate, the chiral dynamics in an APT-symmetric system here can be obtained with the initial state being a waveguide mode. We also experimentally investigated the influences of encircling speed and the EP's position with respect to the encircling loop on the chiral dynamics. We found that a compact system with ∼70 μm length can achieve adiabatic evolution, which is 1 order of magnitude shorter than that of a reported $\mathcal{PT}$-symmetric system [11]. We also found that chiral dynamics disappears when the EP

is outside and far away from the encircling loop. Additionally, we analyzed the dynamical encircling process based on a multimode optical waveguide system and found that the chiral dynamics occurs selectively for different waveguide modes with enhanced robustness against fabrication imperfections, which paves the way for further applications in mode and wavelength switching. The demonstrated *APT*-symmetric system will serve as a new platform for studying topological phases in non-Hermitian topological systems.

Results.—Figure 1(a) illustrates a triple-waveguide system which can be modeled as an *APT*-symmetric system. The three waveguides have different waveguide widths and different effective refractive indices for the propagating light. A metal stripe is fabricated on top of the central waveguide b, causing an additional damping rate γ for the propagating light [see device images in Fig. 1(b)]. If the damping rate is sufficiently high and no light propagates in the central waveguide b, then dissipative coupling between the propagating light in waveguide a and c occurs. Under this condition, the interaction of light between waveguide a and c can be modeled as an *APT*-symmetric system. The simplification process is shown as follows. The Hamiltonian describing the behavior of the propagating light with wave number k_0 in the triple-waveguide system is

$$H_1 = \begin{bmatrix} n_1 k_0 & \kappa_1 & 0 \\ \kappa_1 & n_2 k_0 + j\gamma & \kappa_2 \\ 0 & \kappa_2 & n_3 k_0 \end{bmatrix}, \tag{1}$$

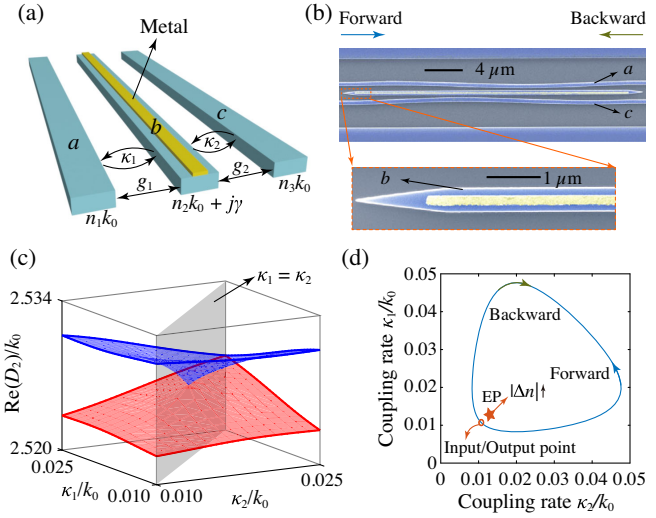

FIG. 1. (a) Illustration of a triple-waveguide system where metal is deposited atop the central waveguide. (b) Scanning electron microscope images of the fabricated triple-waveguide *APT*-symmetric system. The close-up shows the details of the central lossy waveguide. (c) Calculated real part of eigenvalues of the simplified double-waveguide system with Hamiltonian H_2. (d) System's trajectory of dynamical encircling of an EP in the parameter space of the coupling rates κ_1 and κ_2.

where n_1, n_2, and n_3 are the effective refractive indices of waveguide a, b, and c, respectively. κ_1 (κ_2) is the coupling rate between waveguide b and waveguide a (c). Under the conditions of $\gamma \gg k_0|n_1 - n_2|$ and $\gamma \gg k_0|n_2 - n_3|$, the triple-waveguide system can be simplified to a double-waveguide system that consists of only waveguide a and c [23]. Correspondingly, the Hamiltonian is simplified to a 2×2 matrix as

$$H_2 = \begin{bmatrix} n_1 k_0 - j\Gamma_1 & -j\sqrt{\Gamma_1\Gamma_2} \\ -j\sqrt{\Gamma_1\Gamma_2} & n_3 k_0 - j\Gamma_2 \end{bmatrix}, \tag{2}$$

with $\Gamma_1 = |\kappa_1|^2/\gamma$ and $\Gamma_2 = |\kappa_2|^2/\gamma$. Note that for $\Gamma_1 = \Gamma_2$ ($\kappa_1 = \kappa_2$), H_2 in Eq. (2) takes the form of Hamiltonian of *APT*-symmetric systems. The condition of $\Gamma_1 = \Gamma_2 = |\Delta n|k_0$ with $\Delta n = (n_1 - n_3)/2$ corresponds to the EP of the system, which separates the *APT*-broken phase ($\Gamma_1 = \Gamma_2 < |\Delta n|k_0$) from the *APT*-unbroken phase ($\Gamma_1 = \Gamma_2 > |\Delta n|k_0$). Figure 1(c) plots the calculated real part of eigenvalues for the Hamiltonian H_2 of the simplified double-waveguide system with $n_1 = 2.5317$, $n_2 = 2.5270$, $n_3 = 2.5224$, and $\gamma = 0.06k_0$. It is found that the EP only exists for $\kappa_1 = \kappa_2$, and encircling the EP can be achieved by varying the coupling rates κ_1 and κ_2 (see the Supplemental Material for details [26]). Figure 1(d) plots the system's trajectory of dynamical encircling of an EP in the parameter space of the coupling rates κ_1 and κ_2. The dynamical encircling process can be realized by varying the gap g_1 (g_2) between waveguide a (c) and waveguide b. The encircling direction is counterclockwise (clockwise) for forward (backward) propagating light.

We first analyzed the dynamical encircling process with the designed *APT*-symmetric system. Here, we focused on the cases where the initial state is in the *APT*-broken phase with a low damping rate. Figures 2(a) and 2(c) plot the trajectories of state evolution on the Riemann surface with the change of coupling rates in the counterclockwise and clockwise direction of the encircling process, respectively. At the input or output port, the state on the higher (lower) Riemann surface resides mainly in waveguide a (c) and is labeled as state A (B). For the counterclockwise encircling direction, both the initial states A and B end up being state B, as shown in Fig. 2(a). For the clockwise encircling direction, both the initial states A and B end up being state A, as shown in Fig. 2(c). These calculated results show that the chiral dynamics occurs in the designed *APT*-symmetric system. Figures 2(b) and 2(d) plot the amplitudes of eigenstates on the higher (E_h) and lower (E_l) Riemann surface in the counterclockwise and clockwise encircling process, respectively. Take the counterclockwise encircling process as an example, as shown in Figs. 2(a) and 2(b), the initial state A on the higher Riemann surface is converted to state B on the lower Riemann surface after the adiabatic parameter evolution. The initial state B first propagates on the lower Riemann surface and then transits to the higher

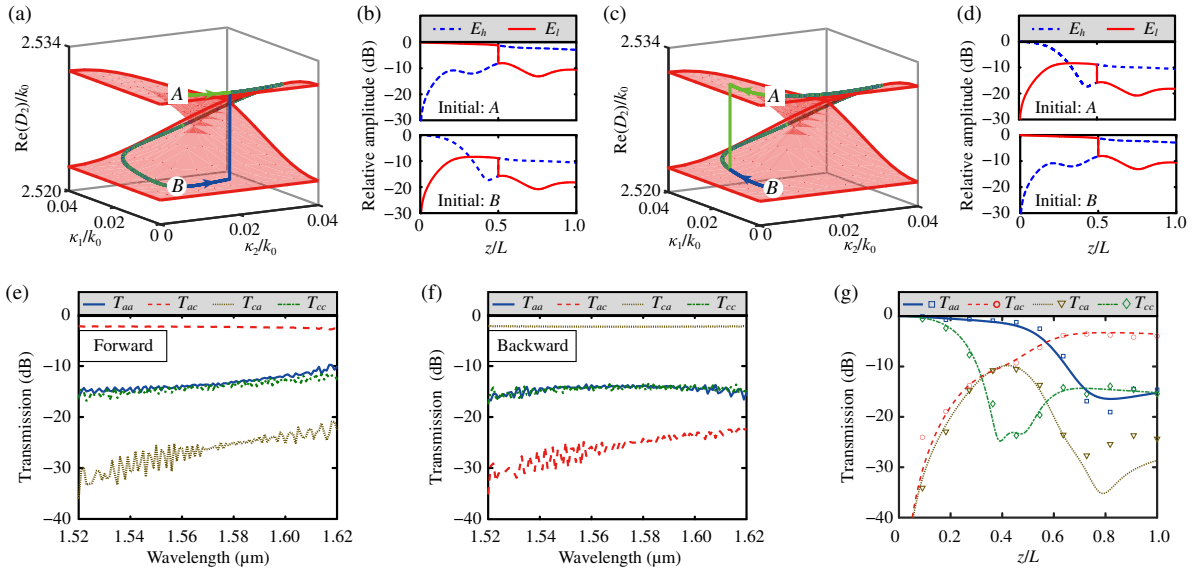

FIG. 2. (a) and (c) Real part of the system's eigenvalues with the curves marking the trajectory of counterclockwise (a) and clockwise (c) encircling starting from state A or B. (b) and (d) Calculated amplitudes of the eigenstates on the respective higher (E_h) and lower (E_l) Riemann surface as a function of the propagation distance in the counterclockwise (b) and clockwise (d) encircling. Upper panel: initial state A. Lower panel: initial state B. (e) and (f) Measured forward (e) and backward (f) optical transmission spectra. (g) Theoretically calculated and experimentally measured optical transmission in waveguide a and c as a function of the propagation distance in the device. Lines: theoretically calculated. Symbols: experimentally measured.

Riemann surface abruptly. The nonadiabatic evolution here is caused by the high damping rate of the eigenstate (see the Supplemental Material for details [26]). Finally, the propagating state returns to state B after an adiabatic evolution. Similar phenomena including the nonadiabatic evolution also occur for the clockwise direction, as shown in Figs. 2(c) and 2(d).

We fabricated the devices and experimentally demonstrated the dynamical encircling process in the proposed system (see the Supplemental Material for details [26]). The waveguide gap at the input port is $g_1 = g_2 = 410$ nm such that the initial state is in the APT-broken phase. Figures 2(e) and 2(f) plot the measured transmission spectra for different propagation directions with the waveguide gap varied around 280 nm. T_{aa} (T_{ac}) and T_{ca} (T_{cc}) represent the normalized transmission from input waveguide a to output waveguide a (c) and that from input waveguide c to output waveguide a (c), respectively. The transmission is dominated by T_{ac} and T_{cc} (T_{ca} and T_{aa}) in the wavelength range of 1.52–1.62 μm for forward (backward) propagating light. The extinction ratio is ∼11 dB at the wavelength of 1.55 μm. Besides, T_{aa} is always similar to T_{cc} irrespective of the propagation direction. It is clear that the dominant transmission is associated with the light propagation direction. Next, we collected more experimental data to analyze the chiral dynamics in this system. Figure 2(g) plots the experimentally measured and numerically simulated optical transmission as a function of the propagation distance for the forward propagating light at the wavelength of 1.55 μm. Starting from state A, the light input to waveguide a is gradually coupled to waveguide c such that the output light resides mainly in waveguide c. The case is more complicated for light input to waveguide c with the initial state B. First, the light is partly absorbed by the metal on top of waveguide b, while the remainder is quickly coupled to waveguide a and experiences a nonadiabatic optical evolution. Then, the light in waveguide a is gradually coupled to waveguide c. The experimental results agree well with the simulated results.

In the above dynamical processes, the initial state is an eigenstate in the APT-broken phase which is similar to the waveguide mode (i.e., the TE_0 mode). However, the eigenstates in the APT-unbroken phase behave differently from the waveguide modes. Since waveguides are a fundamental building block in integrated photonic circuits, it is important to analyze the propagation of waveguide modes in the encircling process. Figure 3(a) plots the forward optical transmission at the wavelength of 1.55 μm as a function of the device length with the waveguide gap varied around 280 nm. The measured results agree well with the calculated results. A larger portion of light input to waveguide a is coupled to waveguide c with an increased device length, and the transmission is finally dominated by T_{ac}. For light input to waveguide c, the transmission is under the effect of chiral dynamics and thus is dominated by T_{cc} for a long device length. A device length of 70 μm is sufficient for adiabatic evolution of the system parameters and for realizing chiral dynamics. Figure 3(b) plots the forward optical transmission at the wavelength of 1.55 μm as a function of the effective refractive index difference Δn

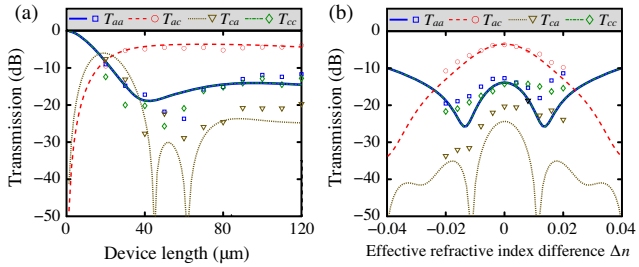

FIG. 3. (a) Theoretically calculated and experimentally measured optical transmission as a function of the device length. (b) Theoretically calculated and experimentally measured optical transmission as a function of the effective refractive index difference Δn. Both (a) and (b) are for the forward propagating light.

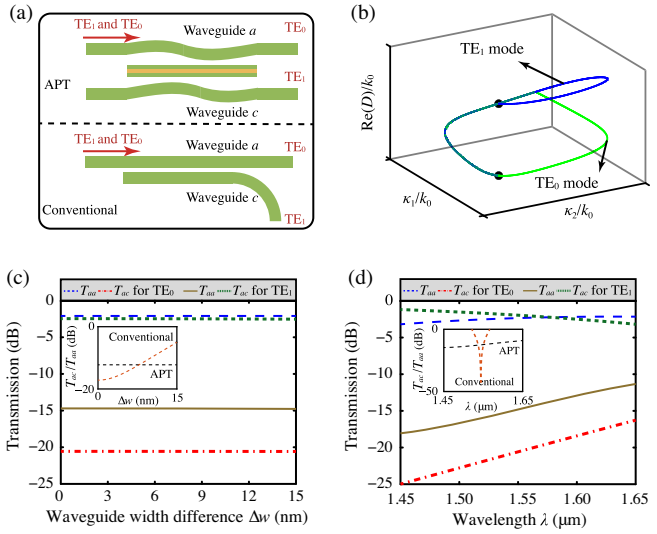

FIG. 4. (a) Illustrations of the proposed *APT*-symmetric and conventional mode (de)multiplexers. (b) Trajectories of the TE_0 and TE_1 modes during the light propagation. (c) Optical transmission of the TE_0 and TE_1 modes as a function of the waveguide width difference Δw. The inset plots the crosstalk of the TE_1 mode for the proposed *APT*-symmetric and conventional mode (de)multiplexers. (d) Optical transmission of the TE_0 and TE_1 modes as a function of the wavelength. The inset plots the crosstalk of the TE_1 mode for the proposed *APT*-symmetric and conventional mode (de)multiplexers.

with the waveguide gap varied around 340 nm. As $|\Delta n|$ increases, the parametric encircling loop is fixed and the EP moves along the diagonal toward the top right direction in Fig. 1(d). For systems with a small effective refractive index difference $|\Delta n|$, the chiral dynamics occurs with the output light residing mainly in waveguide c irrespective of the input waveguide. However, when the effective refractive index difference is relatively large ($|\Delta n| \geq 0.024$), the chiral dynamics does not occur and the output light resides mainly in waveguide a for light input to waveguide a. This is because under this condition the EP is located outside and far away from the encircling loop and light tends to stay in the input waveguide rather than being coupled to the other waveguide.

Finally, we analyzed the dynamical encircling process in the *APT*-symmetric system composed of multimode waveguides and proposed a possible application as shown in Fig. 4(a). We designed the waveguides with waveguide width ~1 μm to support both the TE_0 and TE_1 modes. According to the above analysis, light propagates differently in these modes with adiabatic or nonadiabatic encircling around the EP. The TE_0 mode with smaller coupling rates needs a longer device length for the chiral dynamics than the TE_1 mode. Therefore, with a short device length, the TE_0 mode still propagates in the input waveguide while the TE_1 mode is already coupled into another waveguide. Figure 4(b) shows the trajectories of eigenvalues for the two modes in the dynamical encircling process of the system. Then, based on this system we proposed a mode (de)multiplexer with a device length of 100 μm and the gap varied around 280 nm. Figure 4(c) plots the optical transmission T_{aa} and T_{ac} for both the TE_0 and TE_1 modes at the wavelength of 1.55 μm as a function of the waveguide width difference $\Delta w(= |w_a - w_c|)$. Such a waveguide width difference can be introduced due to imperfect device fabrication. It shows that the proposed system is robust against the waveguide width difference up to 15 nm. For comparison, we also analyzed a mode (de) multiplexer designed under the conventional scheme of directional coupling. It has a length of 110 μm, and consists of two waveguides of the same width separated by a gap of 150 nm. It has different coupling rates for the TE_0 and TE_1 modes, and needs to satisfy the phase-matching condition. Figure 4(c) inset plots the crosstalk of the TE_1 mode for the two types of mode (de)multiplexer as a function of Δw. It is clear that the one based on the proposed *APT*-symmetric system is much more robust against fabrication errors. Additionally, we simulated the optical transmission spectra of the mode (de)multiplexer based on the proposed *APT*-symmetric system, with the results shown in Fig. 4(d). On the shorter wavelength side it has excellent performance, although the crosstalk of the TE_1 mode increases with wavelength. Figure 4(d) inset plots the crosstalk of the TE_1 mode for the two types of mode (de)multiplexer as a function of wavelength λ. It is clear that the one based on the proposed *APT*-symmetric system has a remarkably larger operating bandwidth than the one under the conventional scheme. Therefore, it is expected that dynamically encircling around the EP of an *APT*-symmetric multimode waveguide system will become a new paradigm for mode manipulation with enhanced robustness, which may find new applications in wavelength and polarization splitting on an integrated platform. The demonstrated device structure can also be used for building high-dimensional non-Hermitian topological systems and for exploring quantum optics based on the chiral dynamics.

Conclusion.—In conclusion, we experimentally demonstrated asymmetric mode switching and chiral dynamics in the wavelength range of 1.52–1.62 μm with an extinction ratio of 11 dB with an *APT*-symmetric system on an integrated photonic platform. This system has advantages that it does not require a complicated variation of optical gain or loss rate and it can be fabricated in commercial silicon photonic foundries. In addition, the demonstrated device structure can be harnessed for developing non-Hermitian systems on a chip. For example, the chiral dynamics can still occur for the propagating waveguide modes even if the EP is not inside the encircling loop. Our studies on the effect of different parameters (e.g., device length and effective refractive index difference) on the chiral transmission show that a compact system with the device length of only 70 μm can be used for realizing chiral dynamics. Such a system with the input state being a waveguide mode can easily be integrated with conventional integrated photonic circuits, which paves the way for on-chip non-Hermitian systems. We further proposed a mode (de)multiplexer by harnessing the chiral dynamics which occurs selectively depending on the input optical mode. Compared with conventional mode (de)multiplexers which need to strictly satisfy the phase-matching condition, the proposed multimode system is much more robust against fabrication errors, with a greatly enhanced operating wavelength range. The proposed system sets a new paradigm for mode manipulation by dynamically encircling the EP in integrated photonic circuits, which may inspire further research on the dynamical encircling process in many other branches of physics, such as acoustics and quantum mechanics.

This work was supported by the Research Grants Council of Hong Kong (Project No. 14208717, 14208421).

*Corresponding author.
xksun@cuhk.edu.hk

[1] C. M. Bender and S. Boettcher, Real Spectra in Non-Hermitian Hamiltonians Having $\mathcal{PT}$ Symmetry, Phys. Rev. Lett. **80**, 5243 (1998).
[2] K. G. Makris, R. El-Ganainy, D. N. Christodoulides, and Z. H. Musslimani, Beam Dynamics in $\mathcal{PT}$ Symmetric Optical Lattices, Phys. Rev. Lett. **100**, 103904 (2008).
[3] Z. Feng, J. Ma, and X. Sun, Parity–time-symmetric mechanical systems by the cavity optomechanical effect, Opt. Lett. **43**, 4088 (2018).
[4] H. Hodaei, A. U. Hassan, S. Wittek, H. Garcia-Gracia, R. El-Ganainy, D. N. Christodoulides, and M. Khajavikhan, Enhanced sensitivity at higher-order exceptional points, Nature (London) **548**, 187 (2017).
[5] W. Chen, Ş. Kaya Özdemir, G. Zhao, J. Wiersig, and L. Yang, Exceptional points enhance sensing in an optical microcavity, Nature (London) **548**, 192 (2017).
[6] Z.-P. Liu, J. Zhang, Ş. K. Özdemir, B. Peng, H. Jing, X.-Y. Lü, C.-W. Li, L. Yang, F. Nori, and Y.-X. Liu, Metrology with $\mathcal{PT}$-Symmetric Cavities: Enhanced Sensitivity Near the $\mathcal{PT}$-Phase Transition, Phys. Rev. Lett. **117**, 110802 (2016).
[7] Z. Feng and X. Sun, Giant Enhancement of Rotation Sensing with $\mathcal{PT}$-Symmetric Circular Bragg Lasers, Phys. Rev. Appl. **13**, 054078 (2020).
[8] Z. Feng, J. Ma, Z. Yu, and X. Sun, Circular Bragg lasers with radial $\mathcal{PT}$ symmetry: Design and analysis with a coupled-mode approach, Photonics Res. **6**, A38 (2018).
[9] L. Feng, Z. J. Wong, R.-M. Ma, Y. Wang, and X. Zhang, Single-mode laser by parity-time symmetry breaking, Science **346**, 972 (2014).
[10] A. U. Hassan, B. Zhen, M. Soljačić, M. Khajavikhan, and D. N. Christodoulides, Dynamically Encircling Exceptional Points: Exact Evolution and Polarization State Conversion, Phys. Rev. Lett. **118**, 093002 (2017).
[11] J. W. Yoon *et al.*, Time-asymmetric loop around an exceptional point over the full optical communications band, Nature (London) **562**, 86 (2018).
[12] J. Doppler, A. A. Mailybaev, J. Böhm, U. Kuhl, A. Girschik, F. Libisch, T. J. Milburn, P. Rabl, N. Moiseyev, and S. Rotter, Dynamically encircling an exceptional point for asymmetric mode switching, Nature (London) **537**, 76 (2016).
[13] X.-L. Zhang, T. Jiang, and C. T. Chan, Dynamically encircling an exceptional point in anti-parity-time symmetric systems: Asymmetric mode switching for symmetry-broken modes, Light Sci. Appl. **8**, 88 (2019).
[14] C. Dembowski, H. D. Gräf, H. L. Harney, A. Heine, W. D. Heiss, H. Rehfeld, and A. Richter, Experimental Observation of the Topological Structure of Exceptional Points, Phys. Rev. Lett. **86**, 787 (2001).
[15] T. Gao *et al.*, Observation of non-Hermitian degeneracies in a chaotic exciton-polariton billiard, Nature (London) **526**, 554 (2015).
[16] K. Ding, G. Ma, M. Xiao, Z. Q. Zhang, and C. T. Chan, Emergence, Coalescence, and Topological Properties of Multiple Exceptional Points and Their Experimental Realization, Phys. Rev. X **6**, 021007 (2016).
[17] X.-L. Zhang and C. T. Chan, Dynamically encircling exceptional points in a three-mode waveguide system, Commun. Phys. **2**, 63 (2019).
[18] Q. Zhong, M. Khajavikhan, D. N. Christodoulides, and R. El-Ganainy, Winding around non-Hermitian singularities, Nat. Commun. **9**, 4808 (2018).
[19] L. Ge and H. E. Türeci, Antisymmetric $\mathcal{PT}$-photonic structures with balanced positive- and negative-index materials, Phys. Rev. A **88**, 053810 (2013).
[20] Y. Li, Y.-G. Peng, L. Han, M.-A. Miri, W. Li, M. Xiao, X.-F. Zhu, J. Zhao, A. Alù, S. Fan, and C.-W. Qiu, Anti-parity–time symmetry in diffusive systems, Science **364**, 170 (2019).
[21] P. Peng, W. Cao, C. Shen, W. Qu, J. Wen, L. Jiang, and Y. Xiao, Anti-parity–time symmetry with flying atoms, Nat. Phys. **12**, 1139 (2016).

[22] Y. Choi, C. Hahn, J. W. Yoon, and S. H. Song, Observation of an anti-$\mathcal{PT}$-symmetric exceptional point and energy-difference conserving dynamics in electrical circuit resonators, Nat. Commun. **9**, 2182 (2018).
[23] H. Fan, J. Chen, Z. Zhao, J. Wen, and Y.-P. Huang, Antiparity-time symmetry in passive nanophotonics, ACS Photonics **7**, 3035 (2020).
[24] F. Zhang, Y. Feng, X. Chen, L. Ge, and W. Wan, Synthetic Anti-$\mathcal{PT}$ Symmetry in a Single Microcavity, Phys. Rev. Lett. **124**, 053901 (2020).
[25] H. Zhang, R. Huang, S.-D. Zhang, Y. Li, C.-W. Qiu, F. Nori, and H. Jing, Breaking anti-$\mathcal{PT}$ symmetry by spinning a resonator, Nano Lett. **20**, 7594 (2020).
[26] See Supplemental Material at http://link.aps.org/supplemental/10.1103/PhysRevLett.129.273601 for additional information, which includes Ref. [27].
[27] F. Yang, Y.-C. Liu, and L. You, Anti-$\mathcal{PT}$ symmetry in dissipatively coupled optical systems, Phys. Rev. A **96**, 053845 (2017).